

Non-fitting FLIM-FRET facilitates analysis of protein interactions in live zebrafish embryos

Julia M. T Auer¹ | Laura C Murphy¹ | Dong Xiao²  | David U. Li² | Ann P Wheeler¹ 

¹MRC Human Genetics Unit, Institute of Genetics and Cancer, The University of Edinburgh, Edinburgh, UK

²Department of Biomedical Engineering, University of Strathclyde, Glasgow, UK

Correspondence

Ann Wheeler, MRC Human Genetics Unit, Institute of Genetics and Cancer, The University of Edinburgh, Edinburgh, UK.

Email: ann.wheeler@ed.ac.uk

Abstract

Molecular interactions are key to all cellular processes, and particularly interesting to investigate in the context of gene regulation. Protein–protein interactions are challenging to examine in vivo as they are dynamic, and require spatially and temporally resolved studies to interrogate them. Foerster Resonance Energy Transfer (FRET) is a highly sensitive imaging method, which can interrogate molecular interactions. FRET can be detected by Fluorescence Lifetime Imaging Microscopy (FLIM-FRET), which is more robust to concentration variations and photobleaching than intensity-based FRET but typically needs long acquisition times to achieve high photon counts. New variants of non-fitting lifetime-based FRET perform well in samples with lower signal and require less intensive instrument calibration and analysis, making these methods ideal for probing protein–protein interactions in more complex live 3D samples. Here we show that a non-fitting FLIM-FRET variant, based on the Average Arrival Time of photons per pixel (AAT–FRET), is a sensitive and simple way to detect and measure protein–protein interactions in live early stage zebrafish embryos.

KEYWORDS

confocal microscopy, FRET, live imaging, model organisms

1 | INTRODUCTION

Interactions between proteins, DNA and RNA molecules drive cellular processes, including signal transduction, transcriptional regulation and chromatin organisation. To understand the function of dynamic molecular interactions, they must be characterised with spatial and temporal resolution. This is a particular challenge for complex specimens such as developing embryos or organoids. 3D scanning of thick samples increases image acquisition time, decreasing the temporal resolution to

study interactions. Light scattering increases and photon penetrance decreases proportionally to depth imaged within the sample, reducing signal to noise in the output image. Thick samples can also have artefacts caused by spherical aberration.¹ These can be partially mitigated by use of specialised equipment, such as objectives matched to the refractive index of the sample, resonant scanning or spinning disk confocal microscopy to speed 3D image acquisition, or lightsheet microscopy to improve optical sectioning (Mitchell et al. 2017). We set out to find a technique capable of probing and measuring protein

This is an open access article under the terms of the [Creative Commons Attribution](https://creativecommons.org/licenses/by/4.0/) License, which permits use, distribution and reproduction in any medium, provided the original work is properly cited.

© 2022 The Authors. *Journal of Microscopy* published by John Wiley & Sons Ltd on behalf of Royal Microscopical Society.

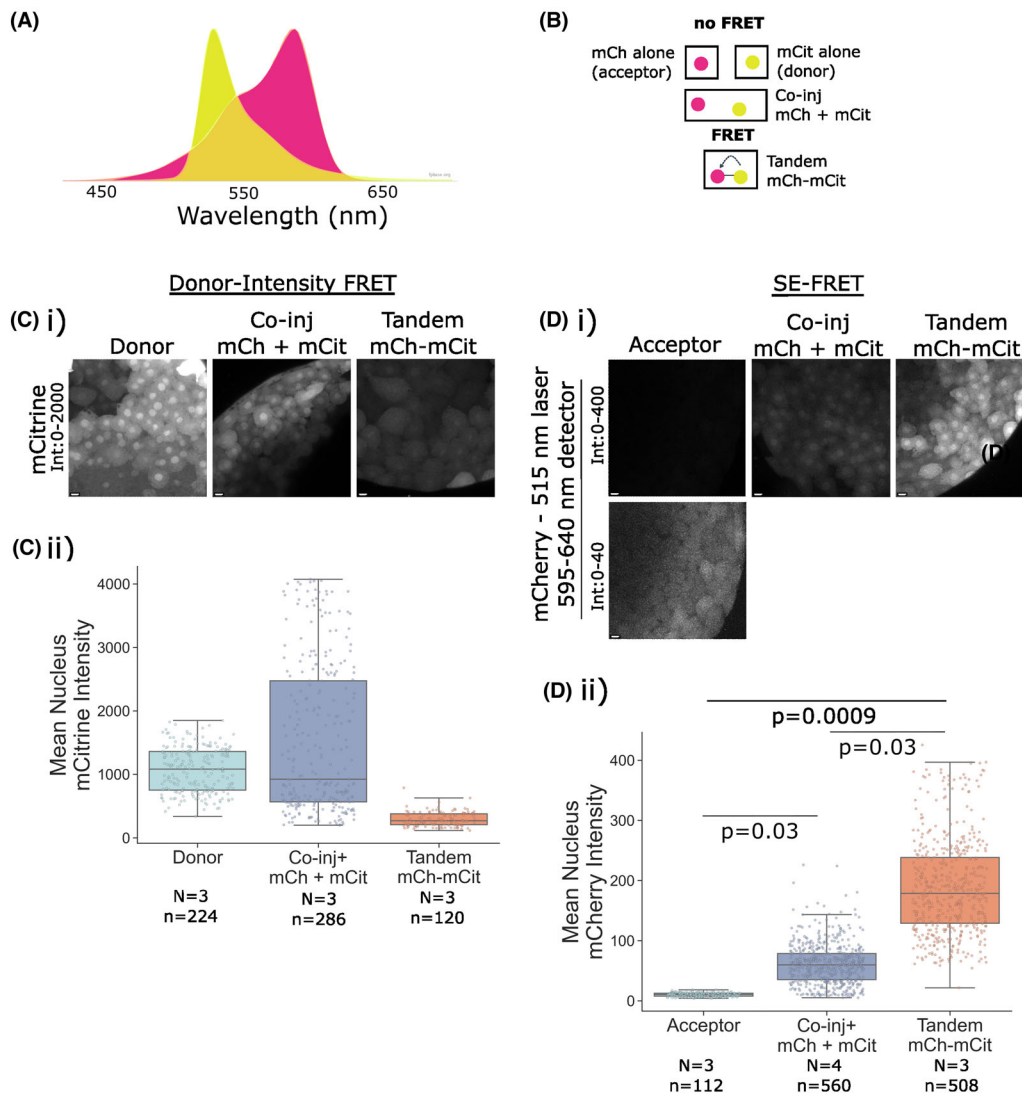


FIGURE 1 Donor intensity FRET and sensitised emission FRET show mCitrine and mCherry is a suitable FRET pair in live early zebrafish embryos. (A) Donor emission (mCitrine, yellow) and acceptor excitation (mCherry, pink) spectra. (B) Conditions compared in FRET and AAT– FRET assays: mCitrine (donor) or mCherry (acceptor) alone. Co-injection of mCherry + mCitrine (Co-inj mCh + mCit), mCherry–mCitrine tandem fusion, with a Glu-Phe linker (Tandem mCh-mCit). Equimolar amounts of mRNA encoding fluorophores were microinjected at the 1-cell stage. (C) Donor intensity FRET assay, embryos expressing of donor alone, Co-inj mCh + mCit, Tandem mCh-mCit. (i) Representative confocal images. (ii) Box and whisker plots of mean nuclear intensities of mCitrine (embryos/condition (N) = 3, nuclei (n) = 120–286, biological replicate (b.r.) = 1). (D) Sensitised emission FRET (SE-FRET) assay (using 515 nm laser and 595–640 nm detector), embryos expressing acceptor alone, Co-inj mCh + mCit, Tandem mCh-mCit. (i) Representative confocal images. (ii) Box and whisker plots of mean nuclear intensities of mCherry (N = 3–4, n = 112–508, b.r. = 1). All images represent maximum intensity projections through the z-stack, scale bar = 10 μ m, Int = displayed intensity range. Data were fit with linear mixed effect models and estimated marginal means compared pairwise.

interactions in a live 3D organism, such as an early zebrafish embryo, which does not require complicated microscope setups and involved analysis.

Two common methods for investigating molecular interactions using confocal imaging are Bimolecular Fluorescence Complementation (BiFC),^{2,3} and Foerster Resonance Energy Transfer (FRET). FRET is the non-radiative energy transfer from an excited donor fluorophore (‘donor’) to an acceptor fluorophore (‘acceptor’) when donor and acceptor are within 10 nm, and the respec-

tive emission and excitation spectra overlap⁴ (Figure 1). Quenching of the donor fluorophore by the acceptor by FRET causes reduction of the donor and increase of the acceptor fluorescence intensity. FRET can therefore be measured by monitoring donor and/or acceptor intensity. The degree of spectral overlap and the donor–acceptor proximity affect the energy transfer efficiency (FRET efficiency).⁵ This means that FRET efficiency can be a measure of the distance as well as the level of interaction between two proteins of interest, when these are

tagged with a donor and an acceptor. However, the relative orientation of donor and acceptor molecules, as well as the refractive index of the medium between them, can also affect the FRET efficiency.^{6,7} FRET can therefore provide real-time measures about two fluorescently tagged interaction partners: stoichiometry, subcellular location, proximity and the degree of interaction and its temporal dynamics (e.g. through the cell cycle).^{6,8–10}

Intensity-based FRET methods include donor intensity FRET, acceptor photobleaching (AccPb) and sensitised emission (SE-FRET). Donor intensity FRET compares the donor intensity in the presence and absence of the acceptor. In AccPb the recovery of donor intensity is measured upon acceptor fluorophore photobleaching.⁶ SE-FRET measures the acceptor intensity (illuminated by a donor-exciting laser) in the presence versus absence of the donor (reviewed in Ref. [8]). However, by quantifying intensities these methods are sensitive to relative concentration and photobleaching. They are also highly dependent on the performance of filters in the microscope system, as spectral bleed-through and autofluorescence can cause misinterpretation of signal readout. Furthermore, aberrations caused by non-uniform sample illumination can affect intensity-based measurements in 3D samples.¹¹ Appropriate controls and robust analysis are therefore required to accurately report FRET efficiency.⁶ These factors make intensity-based FRET assays less suitable for detecting interactions in live 3D samples.

Lifetime-based FRET assays (Fluorescence Lifetime Imaging Microscopy-FRET; FLIM-FRET) are the gold standard for quantitative FRET experiments. Fluorescence lifetime (τ) is the time a fluorophore spends in the excited state, that is, the time between excitation and fluorescent photon emission. τ is not affected by concentration and photobleaching.¹¹ Upon FRET, the donor τ is reduced as the excited donor emits fewer fluorescent photons and spends less time in the excited state. FRET is measured by the reduction in donor τ in the presence and absence of the acceptor. The readout of donor τ allows the fraction of donor molecules interacting with acceptor to be measured. The recovery of donor τ can also be monitored upon AccPb.⁶ Importantly, light scattering in thick samples does not affect fluorescence τ recorded if the delay caused is shorter than the detector time resolution.¹¹ FLIM-FRET is therefore a highly quantitative measure of interactions, and more suitable for live 3D samples.

Measuring τ traditionally uses specialised equipment. Single photon counting detectors are needed to measure when individual photons emitted from a fluorophore arrive at the detector, relative to the excitation of a pulsed laser.¹¹ τ can also be measured in the frequency-domain, but requires a modulated laser and detector.¹² In the time-domain, τ is calculated by fitting the exponential decay of

single photons detected throughout a measurement window by time tagged photon counting, or time correlated single photon counting (TCSPC).¹³ Photons can also be detected in user-defined time intervals with time-gated detectors.¹⁴ In the simplest case, FLIM-FRET fluorescence decay curves are fitted with a bi-exponential model to calculate the τ and fraction of two components: FRETing and non-FRETing donor molecules. However, accurate fitting requires several considerations and intensive computational analysis. For example, the donor's characteristic fluorescence decay may itself be multiexponential and can be affected in donor-acceptor fusions. The instrument's contribution to photon arrival times (Instrument Response Function, IRF) must also be measured and corrected for.¹⁵ TCSPC FLIM-FRET requires high photon counts, dependent on the τ precision and dynamic range and signal-to-noise ratio.¹⁶ For example, photon counts in the order of 10^6 – 10^7 have been reported in cells.^{17,18} Therefore, fitting FLIM-FRET is not ideal to assay dynamic interactions in live 3D organisms with low signal-to-noise ratio.

Non-fitting FLIM-FRET assays have been developed which perform well in lower-signal samples. For example, phasor plots distinguish different populations of molecules, including autofluorescence, FRETing and non-FRETing molecules. For each pixel, the fluorescence decay histogram is transformed to a vector and assigned a point on the phasor plot.¹⁹ This reduces computation, albeit at the cost of some spatial information.²⁰ An even simpler method interrogates the Average Arrival Time (AAT) of photons, which are counted per pixel over the acquisition period. This generates an on-the-fly map of τ -based information which can be used for semiquantitative τ comparisons.²¹ Further to comparing donor τ in the presence or absence of the acceptor to derive FRET efficiency, the minimum extent of interaction can be estimated by converting AAT values to mFD (minimum fraction of interacting donor).^{20,22} This can be visualised directly, or calculated post-acquisition (Leica article²³). AAT-FRET assays are simple to perform since the only calibration required is a negative internal control, the donor alone. As no curve fitting is performed, the precision of AAT measurements is less affected by low photon counts. Time for data collection and processing can therefore be shorter than in TCSPC.

We performed AAT-FRET in live early zebrafish embryos to measure protein-protein interactions. Zebrafish embryos develop quickly, and external fertilisation and development allow easy manipulation and imaging. mRNAs encoding fluorescently tagged proteins of interest are injected at the 1-cell stage, and expression can be observed from approximately 2 h post-fertilisation (2hpf), around Zygotic Genome Activation

(ZGA), reviewed in Ref. (24). Despite the potential of FLIM-FRET to probe dynamic molecular interactions, few have implemented the method to-date in developing zebrafish.²⁵ In this study, we used the Leica Stellaris 8 equipped with GaAsP-Avalanche Photodiode hybrid detectors. In addition to high photon detection efficiency and low (<1.5 ns) detector dead-time, the improved photon counting precision of the new Power Counting technology enhances the single photon counting and dynamic range of Power HyD-X detectors (Leica application note²⁶). This particularly improves imaging sensitivity in samples with low signal-to-noise ratio. Furthermore, combining these detectors with a pulsed white light excitation laser enables analysis of τ of a wide range of fluorophores with a 'standard' confocal configuration and image analysis tools.

We used recent developments in detector sensitivity and on-the-fly image analysis of AAT and mFD to demonstrate that AAT-FRET is an accessible new method to analyse dynamic protein interactions in complex live organisms, such as early zebrafish embryos.

2 | RESULTS

2.1 | mCitrine and mCherry show detectable FRET in live embryos

AAT-FRET requires a high FRET efficiency donor-acceptor pair such as mCitrine and mCherry (Figure 1A). mCitrine, the donor has a high quantum yield at 0.74 and long τ (2.9 ns).²⁷ mCherry has a lower quantum yield at 0.22 and τ (1.6 ns),²⁸ which makes it a good acceptor with low cross-talk.¹¹ To quantify FRET in our system we carried out donor intensity FRET and SE-FRET. We compared the nuclear fluorescence intensities of embryos expressing the donor/acceptor alone, or co-injected mCherry and mCitrine, as negative controls, with a tandem-fused mCherry and mCitrine as a positive control, where donor and acceptor are linked by two amino acids (Glu-Phe) corresponding to an EcoRI site (Figure 1B). Equimolar amounts of mRNA encoding fluorophores were microinjected at the 1-cell stage, and confocal z-stack images of embryos were acquired \sim 3 hpf.

While the mean nuclear mCitrine intensity was lowest in the tandem mCherry-mCitrine, this was not significant ($p = 0.054$, Figure 1C). AccPb-FRET (reviewed in Refs. [6] and [29]) was carried out to confirm FRET, by comparing donor intensity in two z-planes per embryo, pre- vs. post-photobleaching of the acceptor for 30 s. A slight increase in mCitrine intensity was observed in the tandem mCherry-mCitrine (+3.8 a.u., Supplementary Figure 1A and Bi), but this was not significant compared to the co-injected mCherry + mCitrine. This suggests that the sensitivity of

donor intensity FRET to detect interactions in this system is limited.

SE-FRET was used to further characterise these positive and negative controls (Figure 1D). The mean nuclear mCherry intensity, measured by exciting the donor, was lowest for the acceptor alone, increasing for co-injected mCherry + mCitrine ($p = 0.03$), and increasing further for the tandem mCherry-mCitrine ($p = 0.0009$ vs. acceptor alone). While the expression of mCherry, measured by exciting the acceptor directly, was higher for tandem mCherry-mCitrine, the fold-change was much smaller (approx. 2-fold [$p = 0.03$] vs. approx. 17-fold [$p = 0.0009$]) (Supplementary Figure 1E). We also photobleached the donor for 30 s, comparing SE acceptor intensity pre- vs. post-photobleaching, in two z-planes per embryo. The decrease in mCherry intensity was significantly larger in the tandem mCherry-mCitrine than co-injected mCherry + mCitrine ($p = 0.002$, Supplementary Figure 1C and Di). This shows that the tandem mCherry-mCitrine construct undergoes FRET.

Intensity-based FRET assays were difficult to interpret as donor and acceptor intensities were affected by factors other than FRET, such as spectral bleed-through, and low signal penetrance depending on proximity of embryos and nuclei to objective. mRNA microinjection variability, differential mRNA expression, and protein stability could also affect fluorescent protein levels, as seen in the difference in mCitrine expression levels within conditions for donor-intensity FRET (Figure 1C), and mCherry expression between conditions for SE-FRET (Supplementary Figure 1E). This makes precise determination of FRET efficiency difficult. We conclude that mCherry and mCitrine are a suitable FRET pair, but that intensity-based FRET assays are not sensitive or robust enough to measure protein-protein interactions in zebrafish.

2.2 | AAT-based measurements of mCitrine and mCherry reflect expected lifetime values

FLIM uses the change in the τ of the FRET donor as a measure of molecular interactions (Figure 2A). As mentioned previously, this is a more robust measure of FRET, which does not depend on fluorescence intensity, and is not affected by photobleaching. However, traditional fitting FLIM-FRET was not suitable for our system. The fast 15- to 20-min cell cycle³¹ and large volume of zebrafish embryos are not compatible with the long acquisition time per image which would be required to collect sufficient photons for TCSPC FLIM-FRET due to the low signal-to-noise ratio.¹⁶

Therefore, we investigated a recent implementation of non-fitting FLIM, which allows faster image acquisition

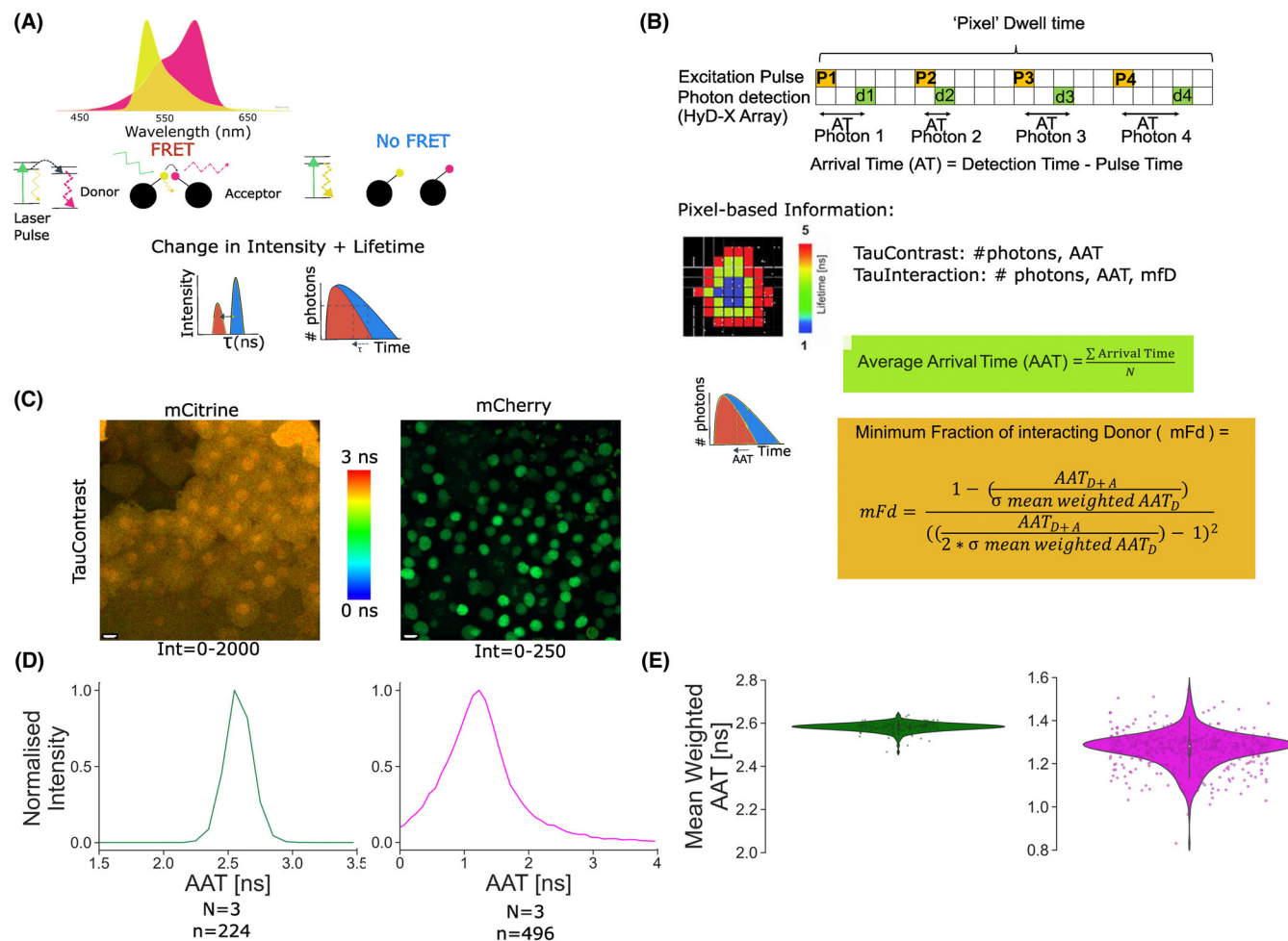


FIGURE 2 Average pixel arrival time (AAT) values for mCitrine and mCherry reflect expected fluorescence lifetime values. (A) Schematic of how AAT-FRET works. (B) Schematic of AAT, describing how AAT and minimum Fraction of Donor interaction (mFd) are calculated. (C) Representative confocal images of mCitrine and Sox19b-mCherry) acquired in TauContrast mode, giving AAT and intensity values per pixel. Images represent maximum intensity projections through the z-stack, scale bar = 10 μm . (D) Lineplots of AAT versus the summed intensities of pixels with each AAT value, averaged and normalised per condition, for nuclei expressing mCitrine or Sox19b-mCherry. (E) Violin plots comparing nuclear mean weighted AAT for mCitrine ($N = 3$, $n = 224$, b.r. = 1) and mCherry ($N = 3$, $n = 496$, b.r. = 1).

by requiring lower photon counts, ~ 100 photons per pixel.^{18,20} In AAT-FRET, the average arrival time of photons (AAT) is recorded per pixel, with a resolution of 0.1 ns (Leica application note²¹) (Figure 2B, Section 4). mCitrine has a high τ of 2.9 ns which lowers by 0.15 - 0.75 ns in the presence of an mCherry-tagged interaction partner or a tandem fusion.²⁷ The difference in τ between FRETing and non-FRETing donor, and of the acceptor mCherry (1.6 ns) is larger than the 0.1 ns detector resolution, making mCitrine-mCherry an ideal FRET pair for AAT-FRET.

Since τ is affected by conditions including the pH, temperature, viscosity and medium polarity (described in Ref. [31]), and AAT may further differ from τ values due to the calculation method,²⁰ AATs in our system may differ to published values. We therefore characterised the donor and acceptor AAT of our chosen FRET pair in live early zebrafish embryos. AATs were measured on a confocal

system fitted with high sensitivity photon counting detectors and a pulsed white light laser (Section 4). mCitrine and a Sox19b-mCherry fusion mRNA were microinjected separately into 1-cell stage embryos. Z-stack images were acquired in TauContrast mode (Leica Microsystems), at 8 μm intervals, for 3 embryos per condition (Figure 2C). This provided intensity and an AAT values for each pixel (Figure 2B). These were converted to lineplots of AAT versus the summed intensities of pixels with each AAT value, averaged and normalised per condition (Figure 2D, Section 4). The mean weighted AAT for mCitrine and Sox19b-mCherry were on average 2.58 ns for mCitrine and 1.27 ns for mCherry, slightly lower than literature values (2.9 ns and 1.6 ns respectively) (Figure 2E and Table 1).²⁷ Taken together, this shows that mCitrine and mCherry are a suitable FRET pair and that AAT is fast and sensitive enough to facilitate lifetime-based data acquisition across the developing zebrafish embryo in 3D.

TABLE 1 Comparison of AAT values measured (Figure 3) and fluorescence lifetime (τ) values reported in Ref. (27) for Stx3-mCitrine and Ref. (28) for mCherry

Fluorescent protein	Lifetime reported in literature (ns)	Measured lifetime (ns)
mCitrine	2.90	2.58
mCherry	1.6	1.27

TABLE 2 Image acquisition time and pixel dwell time for acquisition parameters tested, times given to 3 sig. fig. (\pm standard deviation)

Condition for point scanning	Acquisition time /image (s)	Pixel dwell time (μ s)
Pixel array (area sampled)	128 \times 128 (1.56 μ m ²)	30.80
	256 \times 256 (0.79 μ m ²)	15.40
	512 \times 512 (0.40 μ m ²)	7.69
Scan speed	100 Hz	30.80
	200 Hz	
	400 Hz	6.34
Line accumulation	4	15.40
	8	
	16	15.40
Pinhole size	1 AU	15.40
	2 AU	

2.3 | Optimisation of spatial resolution, acquisition speed and photon counts for AAT– FRET

Having chosen a suitable FRET pair, we optimised acquisition parameters to detect dynamic nuclear interactions by AAT– FRET in rapidly developing zebrafish embryos. At ZGA (\sim 3 hpf), these have large nuclei, approximately 13–14 μ m diameter,³¹ and short cell cycles (15–20 min²⁹). To capture as many nuclei as possible per embryo within a single cell cycle, spatial and temporal resolution need to be balanced with sufficient photon counts for precise AAT measurements.

A high 1.2 numerical aperture objective was selected to provide a large enough working distance to focus on nuclei at different depths. Water immersion was used to minimise artefacts caused by refractive index mismatch to zebrafish nuclei. 1.44 \times digital magnification was chosen so that the embryo filled the field of view. For preliminary analysis, single z-plane images of embryos expressing co-injected mCherry + mCitrine were acquired in TauContrast mode, varying the pinhole size, pixel array, scan speed and line accumulation (Supplementary Figure 2). The precision of AAT values measured per nucleus versus image acquisition time was assessed by comparing pixels per nucleus, intensity per nucleus, AAT lineplots and standard deviation of mean weighted AAT, pixel dwell time and image acquisition time (Figure 3A and B, Table 2 and Supplementary Table 1). Fewer larger pixels increased photon counts

per pixel and thereby AAT precision (Figure 3A and B and Supplementary Table 1) and decreased the acquisition time almost twofold (Table 2). However the resolution achieved using the largest pixels (128 \times 128, 1.6 μ m²) was too low to give useful spatial information in nuclei of 13–14 μ m diameter. Slower scan speeds and increased line accumulation also improved AAT precision by increasing photons collected per pixel (Figure 3A and B and Supplementary Table 1), but slower scanning increased acquisition times almost twofold, to 8 s per image (Table 2). Line accumulation minimally affected acquisition time (Table 2).

Since we could not acquire 3D information at Nyquist resolution within the 15- to 20-min cell cycle, we decided that opening the pinhole and acquiring a larger optical section would enable more precise AAT measurements, as more photons per pixel could be collected, without compromising the axial resolution (Figure 3A and B and Supplementary Table 1). For these studies the intermediate 256 \times 256 pixels, 200 Hz, 8-line accumulation, and the larger 2 Airy Unit (AU) pinhole were selected, as a compromise between precise AAT measurements, spatial resolution and acquisition time (Figure 3C). These settings also achieved the recommended pixel dwell time of \sim 15 μ s (Table 2).¹⁴ DNA was labelled with SiR-DNA dye to enable semiautomated segmentation of nuclei (Figure 3D). Variable or diffuse SiR staining could result from nuclear export,³³ cell cycle stage desynchronisation at ZGA,²⁴ and post-ZGA establishment of compact heterochromatin in zebrafish.³⁴

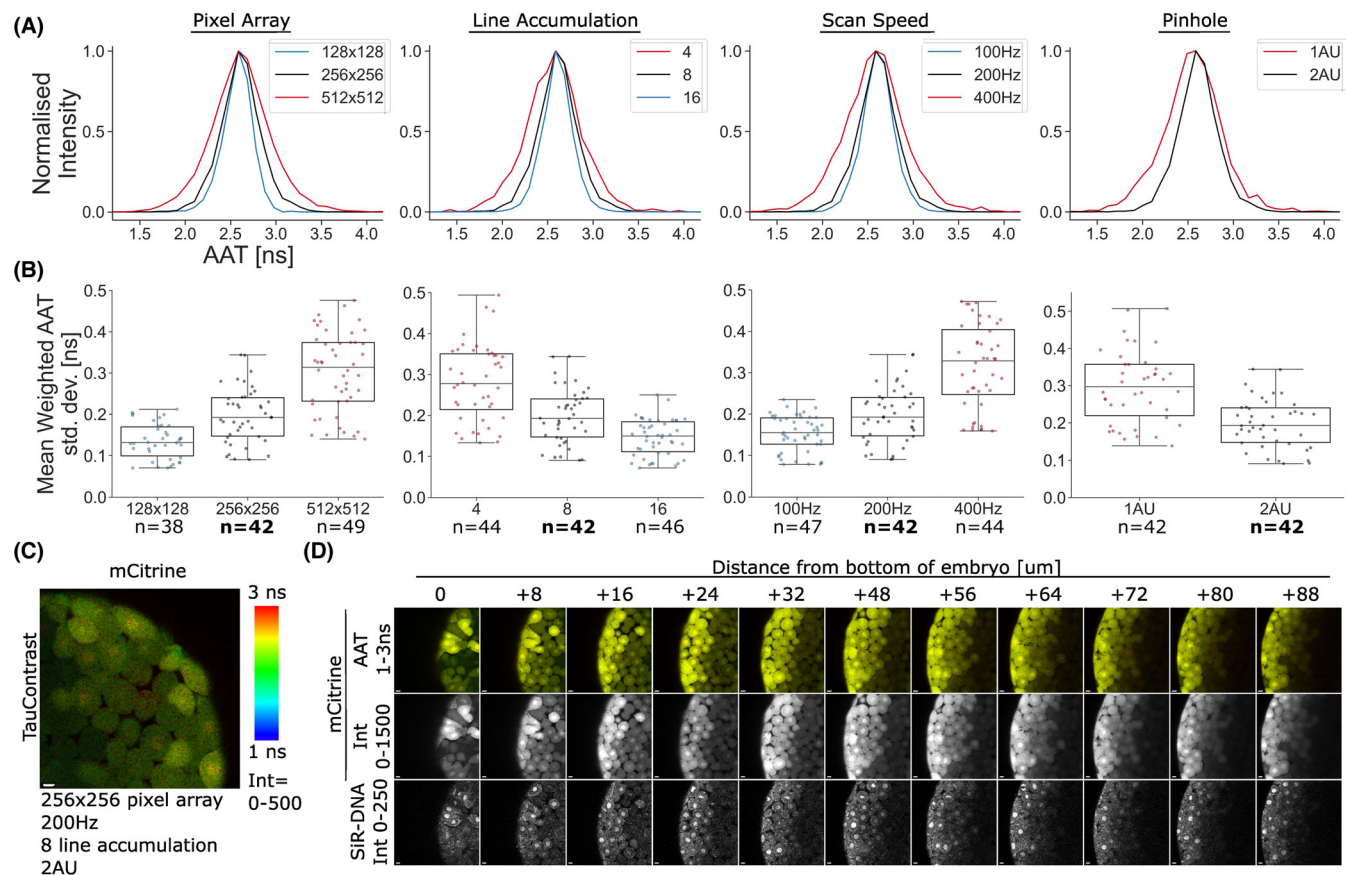


FIGURE 3 Optimisation of acquisition parameters for mCitrine TauContrast images. (A, B) Pixel array, line accumulation, scan speed, and pinhole size were varied, with baseline settings of 256×256 px, 200 Hz, 8 line accumulation, 2AU, in embryos expressing co-inj mCh + mCit. (A) Average nuclear AAT lineplots, from single z-plane images were acquired in TauContrast mode. (B) Box and whisker plots of standard deviation of mean weighted AAT per nucleus ($N = 3$, $n = 38$ – 49 , bold = baseline, b.r. = 1). (C) Representative single z-plane TauContrast image of optimised acquisition parameters. (D) Z stack through a representative AAT data set taken from zebrafish embryo expressing mCit, Z step = $8 \mu\text{m}$. Top to bottom: mCit Taucontrast image, mCit intensity, SiR-DNA intensity. Scale bar = $10 \mu\text{m}$, Int = displayed intensity range, AAT = displayed AAT range.

Finally, given the slow image acquisition times (5–5.5 s per z-plane, Table 2) and large z-volume ~ 40 – $70 \mu\text{m}$ – depending on embryo orientation – a compromise between spatial and temporal resolution also had to be made in the z-axis. $8 \mu\text{m}$ z sections were chosen (Figure 3D). In summary, confocal acquisition parameters were varied to find settings giving the highest photon counts and lateral resolution for the nucleus ROIs, while minimising acquisition time and photodamage to enable as many optical sections through the developing embryo to be collected within the short cell cycle.

2.4 | AAT-based measurements detect FRET in live embryos

We then tested the sensitivity of AATs measured in Tau-Contrast mode to detect protein–protein interactions in our system, using the same fluorophore controls as pre-

viously (Figure 1B). The calculated mean weighted AAT of mCitrine decreased by 0.16 to 2.44 ns on average in zebrafish nuclei expressing tandem mCherry–mCitrine versus the donor alone ($p < 0.0001$, Figure 4B). The mean weighted AAT of mCitrine in the presence of co-injected mCherry did not change significantly compared to mCitrine alone. This indicates that our system is sensitive enough to detect FRET between mCitrine and mCherry (Figure 4A and B).

AccPb provided additional evidence that AAT measurements detect changes in lifetime due to FRET (Figure 4C–E). We observed that the mean weighted AAT of the donor increased slightly within nuclei by 0.022 ns on average upon AccPb, for the tandem mCherry–mCitrine (Figure 4D, $p = 0.01$). This was a significantly larger change in mean weighted AAT than for co-injected mCherry + mCitrine ($p = 0.01$, Figure 4C–E). This verified that FRET can be detected by measuring the change in mCitrine AAT.

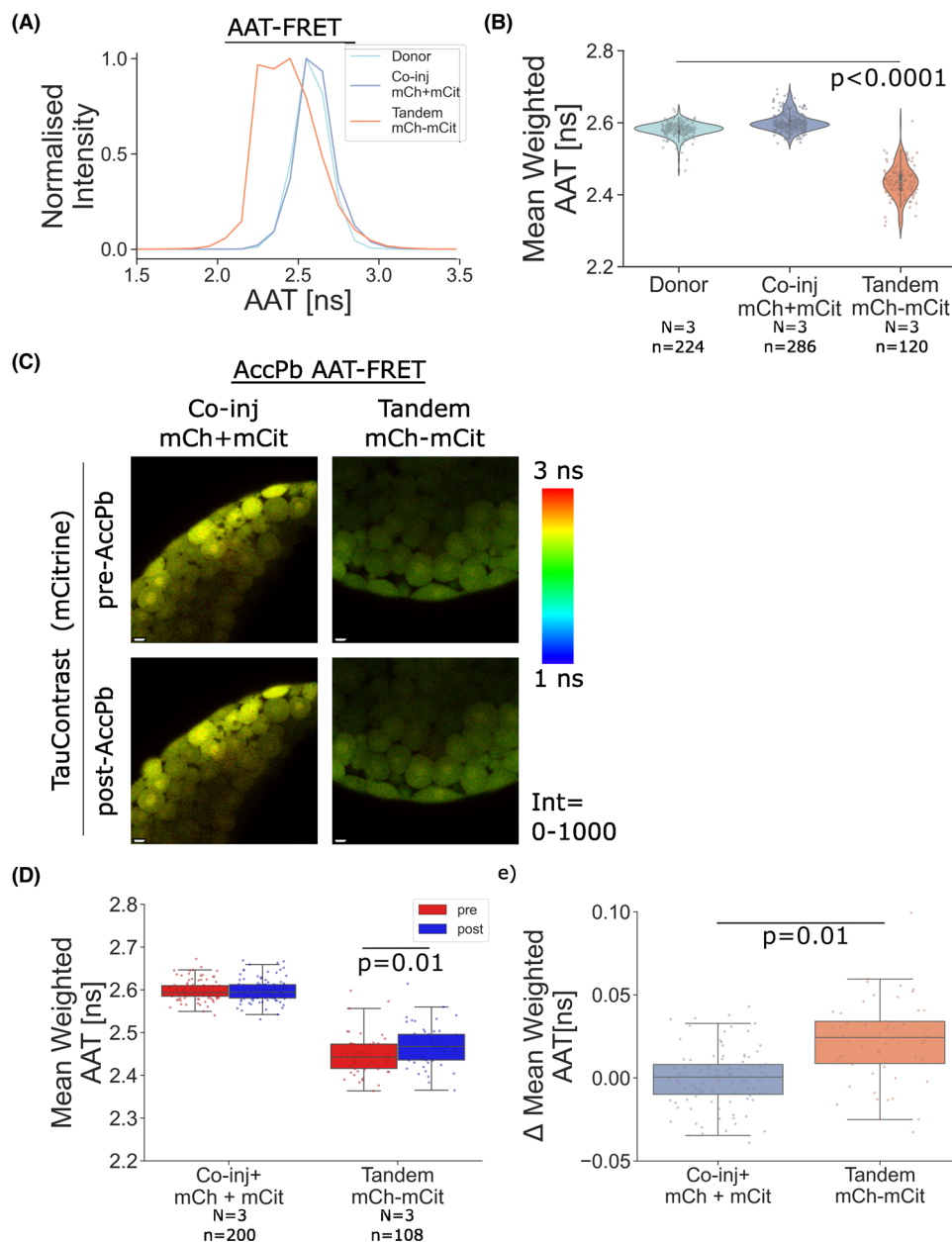


FIGURE 4 AAT-FRET can detect protein interactions in live zebrafish embryos. (A) Average nuclear mCit AAT lineplots from z-stacks acquired in TauContrast mode. (B) Violin plots showing mCit mean weighted AAT per nucleus ($N = 3$, $n = 120$ – 224 , b.r. = 1). (C) AccPb AAT-FRET assay: Pre- and post-AccPb images were acquired in TauContrast mode after z-stacks, for two z-planes in the same embryos used for AAT-FRET. Representative single z-plane TauContrast confocal images of donor channel pre- and post-AccPb, scale bar = $10 \mu\text{m}$, Int = displayed intensity range. (D) Box and whisker plot of mean weighted AAT pre- vs. post-AccPb, for individual nuclei ($N = 3$, $n = 108$ – 200 , b.r. = 1). (E) Box and whisker plot of difference (Δ) in mean weighted AAT pre- vs. post-AccPb, for individual nuclei. Data were fit with linear mixed effect models and estimated marginal means compared pairwise.

2.5 | AAT-based minimum fraction of donor interaction (mfD) can estimate degree of donor-acceptor interaction in live zebrafish embryos

An estimate of donor-acceptor interaction, mfD, was calculated by comparing the AAT of the donor alone, versus in the presence of an acceptor²⁰ (Section 4). Data

were collected using TauContrast mode for z-stacks and TauInteraction mode for individual z-plane images (Figure 5C). TauInteraction is an implementation of the mfD metric^{20,23} and provides an mfD value per pixel in addition to intensity and AAT value. TauInteraction mode was used for on-the-fly image analysis and representative images (Figure 5C). AATs acquired in TauContrast mode were used to calculate mfD values values per pixel,

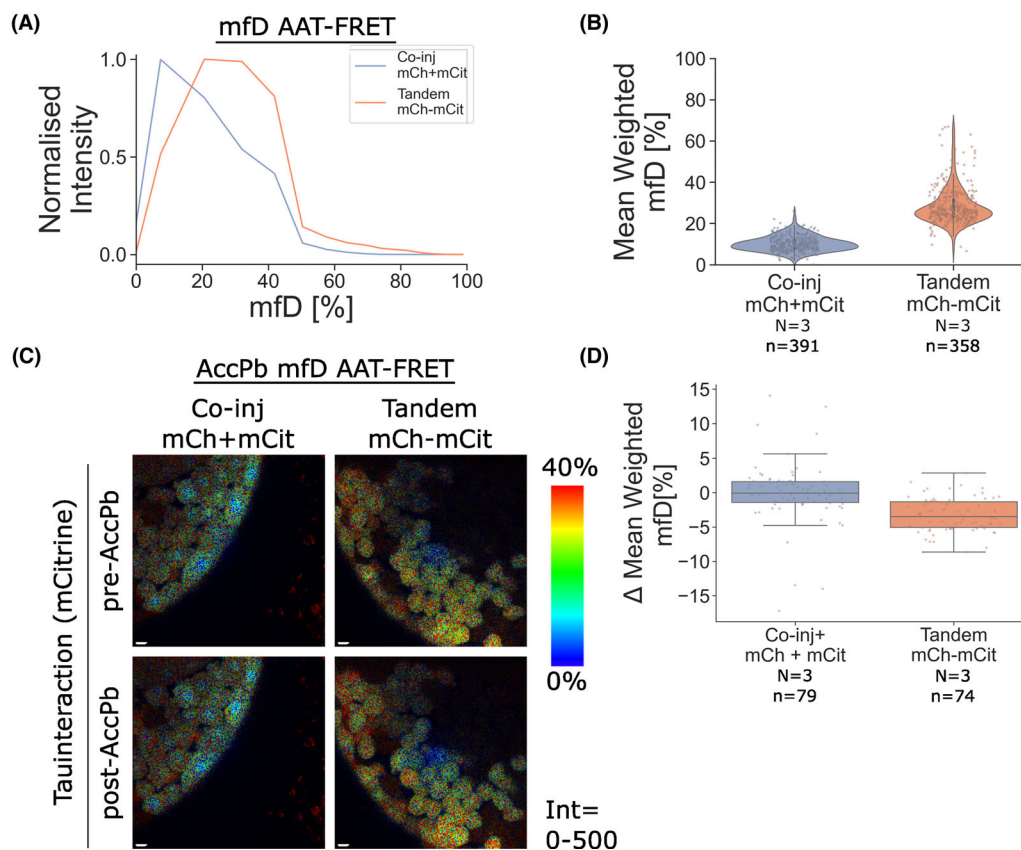


FIGURE 5 AAT-based minimum fraction of interacting donor molecules (mfD) can estimate degree of donor–acceptor interaction in live zebrafish embryos. (A) Average nuclear mfD lineplots converted from AAT values from z-stacks acquired in TauContrast mode. The mfD was calculated from AAT values per pixel, compared to the average mean weighted AAT of the donor alone (Section 4). (B) Violin plots showing mean weighted mfD per nucleus ($N = 3$, $n = 358$ – 391 ; donor alone calibration $N = 1$, $n = 133$, b.r. = 1). (C) AccPb AAT– FRET assay: pre- and post-AccPb images were acquired for mCit in TauInteraction mode after z-stacks, for two z-planes in the same embryos used for AAT FRET. Representative single z-plane TauInteraction confocal images of mfD pre- and post-AccPb, scale bar = $10 \mu\text{m}$, Int = displayed intensity range. (D) Box and whisker plot of difference (Δ) in mean weighted mfD pre- vs. post-AccPb, for individual nuclei ($N = 3$, $n = 74$ – 79 , b.r. = 1)

post-acquisition. The average mean weighted AAT for the donor alone (2.6 ns) was used to convert AAT to mfD (Figure 5A). By calculating the mean weighted mfD, we estimated that on average 27.9% of donor molecules are interacting with acceptor molecules in embryos expressing the tandem mCherry–mCitrine, versus 8.4% in co-injected mCherry + mCitrine (Figure 1B). This is in the same range as the 27–29% mfD reported for an eGFP–mCherry fusion.^{23,34} As mfD underestimates the degree of molecular interaction,²² this indicates that our mCherry–mCitrine construct shows a high degree of FRET efficiency, which can be detected by AAT– FRET in live zebrafish embryos.

AccPb was carried out as previously described, by comparing the mean weighted mfD of individual nuclei pre- versus post-AccPb (Figure 5C and D). The mean weighted mfD of the tandem mCherry–mCitrine decreased by -5.11% on average, versus an increase of 0.96% for co-injected mCherry + mCitrine (Figure 5D). This is in line with tandem mCherry–mCitrine undergoing FRET.

In summary, we show that using AAT– FRET and estimated mfD measures the degree of protein–protein interactions in live early stage zebrafish embryos.

3 | DISCUSSION

Here, we show the application a τ -based FRET assay, AAT– FRET and mfD²⁰ and analyse protein–protein interactions in live 3D organisms with low signal-to-noise ratios. AAT– FRET does not require instrument calibration, definition of donor τ decay characteristics or time-intensive photon decay fitting or computation to analyse protein interactions. A further advantage is faster acquisition times compared to TCSPC FLIM. Using the built-in software, it is also possible to qualitatively assess AAT and mfD on-the-fly using the TauContrast and TauInteraction modes.

We outline considerations, optimisation of acquisition parameters and controls for AAT– FRET assays to detect

and measure interactions in early zebrafish embryos. We verified that mCitrine and mCherry are a suitable FRET pair in this system by intensity-based FRET assays (Figure 1, Section 4) and validated this using AccPb (Supplementary Figure 1). We then showed that τ -based AAT values are comparable to literature τ values for mCitrine and mCherry (Figure 2) to ensure that mCitrine and mCherry can be used to interrogate interactions by τ -based AAT–FRET in live zebrafish embryos. Finally, we showed, using the Stellaris 8 TauSense tools, that AAT–FRET and derived estimate of interaction extent (mfD) can detect interactions in a control tandem mCherry–mCitrine protein expressed in early zebrafish embryos (Figures 4 and 5). Others have reported marginally larger τ changes for mCitrine–mCherry in FLIM-FRET experiments to measure Stx3-VAMP3 interactions in dendritic cells.²⁷ We note that τ and changes due to FRET depend on the cellular environment and the calculation method.²⁰ Different linkers affecting mobility of fluorophore tags may also define the probability of FRET to occur between tags of interacting proteins.

The difference in fluorescence characteristics between the tandem mCherry–mCitrine, the co-injected mCherry + mCitrine and donor/acceptor alone controls was more pronounced in AAT–FRET (Figures 1C and D and 4A–C and Supplementary Figure 1). We found that the mCitrine AAT decreased by 0.16 ns ($p < 0.0001$, Figure 4B) and estimated a minimum of 27.9% donor molecules interacting with acceptor molecules (Figure 5B), in the tandem mCherry–mCitrine compared to the donor alone. We used AccPb to verify these differences were due to FRET in the tandem fusion. We showed that the mCitrine AAT recovered by 0.022 ns ($p = 0.01$, Figure 4D and E) within nuclei in the tandem mCherry–mCitrine compared to the donor alone, and fewer donor molecules interacted (–5.11%, Figure 5C and D). We conclude that AAT–FRET assays are sensitive enough, and more robust than intensity-based FRET assays, which are affected by variability in relative donor and acceptor expression levels, for the investigation of protein–protein interactions in zebrafish embryos.

This non-fitting approach does have trade-offs compared to TCSPC FLIM-FRET: AAT–FRET collects τ data of a population of photons per pixel rather than per photon, so the ability to resolve τ populations is limited by the 0.1 ns AAT resolution. The mfD measure is an underestimate of donor–acceptor interaction,²² additionally limited by the AAT resolution. In the current configuration of our instrument, detecting AAT–FRET is therefore limited to FRET pairs for which the donor τ reduction is greater than 0.1 ns. Lower photon counts still affect the precision of measured AAT values (Figure 3 and Table 1). The number of photons collected can be affected by protein expression levels, embryo orientation and proximity to the objective.

τ values may also vary between samples due to differences in the environment such as pH and temperature,¹¹ causing variability in AAT measurements between embryos or experimental days. Use of an internal control for each biological replicate, such as the AAT of the donor alone, is therefore necessary.

Furthermore, photobleaching for AccPb assays in zebrafish embryos was challenging as the light intensity decreases drastically throughout the sample. More effective photobleaching (see Supplementary Figure 1) would require assaying individual nuclei with increased magnification, which would however slow overall acquisition time for assaying multiple nuclei within each embryo. In addition to this, AccPb is an end-point assay, and therefore cannot be used to investigate dynamic interactions. The timescale of each measurement cycle (approximately 40 s for our individual z-planes) is not comparable to dynamic protein interactions.

AAT–FRET is an excellent method, which facilitates investigation of the spatial and temporal dynamics of molecular interactions in live complex organisms. Zebrafish embryos in particular offer a quick and simple system to measure interactions due to their ease of manipulation and fast expression of mRNA microinjected proteins from 2 hpf. We would expect that further enhancement in detector sensitivity and development of methods such as light-sheet FLIM-FRET³⁵ would lead to methods such as AAT–FRET being used more widely and could mitigate the need for compromising acquisition parameters, such as optical sectioning, as was necessary for this work (Figure 3). Overall, AAT–FRET is a suitable method to semiquantitatively measure protein interactions in live 3D samples.

4 | MATERIALS AND METHODS

4.1 | mRNA microinjections and embryo mounting for imaging

Zebrafish were maintained in accordance with UK Home Office regulations, UK Animals (Scientific Procedures) Act 1986, amended in 2013 and European Directive 2010/63/EU under project license 70/8000 and P8F7F7E52. All experiments were approved by the Home office and AWERB (University of Edinburgh Ethics Committee). Fish stocks used were: Maternal-zygotic Nanog-null (MZnanog^{-/-}). Adult fish were maintained at ~28.5°C under 14:10 light:dark cycles. Embryos were kept at 28.5°C in embryo medium (E3) and staged according to the reference table provided by Kimmel and colleagues (Kimmel et al., 1995). mRNA was made by in vitro transcription of pCS2+ constructs (sp6 mmessage mmachine kit, Invitrogen).

Embryos were microinjected at 1-cell stage with equimolar amounts of mRNA (95 pg mCherry, 97 pg mCitrine, 192 pg mCherry–mCitrine), and SiR-DNA (Spirochrome) at a final concentration of 174 μ M, in 500 pL. Embryos were manually dechorionated 1 h post-fertilisation (hpf), prior to mounting in low-melting-point agarose (0.7% in E3). Imaging was carried out \sim 3 hpf (1000-cell stage) at 26.5°C.

4.2 | Confocal imaging including FRET

AAT and confocal imaging was carried out on a Leica Stellaris 8 Confocal Microscope with White Light Laser (WLL), HyD-X and HyD-S detectors and a 40 \times 1.2 NA water-immersion objective lens. AAT FRET images were acquired using the Stellaris 8 TauSense tools, (<https://media.nature.com/original/magazine-assets/d42473-020-00364-w/d42473-020-00364-w.pdf>).

Image data were acquired in Frame Sequential mode. For intensity-based and AAT– FRET, donor (mCitrine) and SiR-DNA were imaged to create a z-stack with an 8- μ m z-step size, using the 515 nm laser at 40% power with a HyD-X detector (523–570 nm), and the 652 nm laser at 20% power with a HyD-X detector (digital mode, 662–710 nm), respectively. To verify protein expression levels, pre-acquisition images were taken for a single z-plane per embryo, using the 515 nm laser at 30% power for mCitrine (HyD-detector, 523–570 nm), using the 587 nm laser at 30% power for mCherry (HyD-detector, 595–640 nm) and using the 652 nm laser at 20% power laser for SiR-DNA (HyD-X detector, digital mode, 662–710 nm).

Acceptor photobleaching was carried out for two z-planes on opposite ends of the z-stack. The acceptor (mCherry) was bleached using 100% 587 nm laser for 30 s. Pre- and post-bleach images were acquired with same settings as above for mCitrine and SiR-DNA, and an additional channel to monitor mCherry intensity: 30% 587 nm laser with HyD detector (595–640 nm).

For intensity-based FRET, the the HyD-X detector was used in photon counting mode. For AAT– FRET, the HyD-X detector was used in TauContrast mode (Intensity and AAT value given per pixel). For AAT– FRET Acc-Pb, the HyD-X detector was used in TauInteraction mode (Intensity, AAT and mfD value given per pixel).

For SE-FRET, acceptor (mCherry) and SiR-DNA were imaged to create a z-stack with an 8- μ m z-step size, using the 515 nm laser at 40% power with a HyD-X detector (TauContrast mode, 595–640 nm), and 652 nm laser at 20% power with a HyD-X detector (digital mode, 662–710 nm), respectively. Pre-acquisition images were acquired as for intensity-based or AAT– FRET. Donor photobleaching

was carried out for two z-planes on opposite ends of the z-stack. The donor (mCitrine) was bleached using the 515 nm laser at 100% power with a laser for 30 s. Pre- and post-bleach images were acquired with same settings as above for mCherry and SiR-DNA, and an additional channel to monitor mCitrine intensity: 515 nm laser at 30% power with a with HyD detector (523–570 nm).

4.2.1 | Image analysis

Images were processed in Fiji (ImageJ)³⁶ or LAS-X (Leica Microsystems). 3D nuclear segmentation was carried out in Fiji after background removal and Gaussian blur filter in the SiR-DNA channel, and the resultant regions of interest (ROIs) were used to interrogate the mCitrine–mCherry intensity/AAT channels. For some images, mCitrine/mCherry intensity channels were used to verify/carry out segmentation. Background subtraction using a rolling ball radius of \sim 10 pixels and Gaussian blur of \sim 0.9 μ m were performed on the SiR-DNA channel (settings varied for embryos with different SiR-DNA signal patterns). The resultant stack was used to perform 3D nuclear segmentation was carried out using Trackmate with the built-in StarDist detector (Ershov et al. 2022). 2D ROIs representing segmented nuclei detected on each z-planes were filtered by manual thresholding of radius, signal-to-noise, and quality features, as well as manual inspection to remove false detections. The remaining detections were linked together using the Trackmate overlap tracker to create a 3D label stack, which was used to extract the pixel intensity and AAT values for each nucleus from original image stack using the 3D ImageJ Suite.^{36,37} For single z-planes pre-/post-bleach images, nuclei were segmented manually (Fiji or LAS-X), and pixel intensity and AAT values were extracted for each nucleus.

4.2.2 | Data processing

Nucleus ROI data from Fiji processing, giving an intensity and AAT value per pixel were imported into Python³⁸ and processed using Pandas³⁹ and NumPy.⁴⁰ Plots were made using Seaborn.⁴¹ Pixels were binned into 0.1 ns AAT bins (matching the detector resolution), and pixel intensities for each AAT bin summed, creating an AAT versus intensity plot for individual ROIs. These match the AAT plots imported from nuclei segmented in LAS-X. AAT plots were normalised to an intensity of 1, averaged across each condition and re-normalised to create line graphs for visual comparison. The mean-weighted AAT per nucleus was calculated from individual ROI AAT plots using the

calculation:

$$\text{Mean weighted AAT} = \frac{\sum \left(\text{AAT} \times \frac{I}{I_{\max}} \right)}{\sum \left(\frac{I}{I_{\max}} \right)},$$

where I is the Intensity at a given AAT (sum of photons counted in pixels with given AAT) and I_{\max} is the maximum Intensity value for a given ROI.

mfD was calculated per pixel from AAT values. Mean weighted mfD was calculated as for Mean Weighted AAT.

$$\text{mfD} = \frac{1 - \left(\frac{\text{AAT}_{D+A}}{\sum \text{mean weighted AAT}_D} \right)}{\left(\left(\frac{\text{AAT}_{D+A}}{2 \times \sum \text{mean weighted AAT}_D} \right) - 1 \right)^2}.$$

mfD and mean weighted mfD values <0 were set to 0, as the minimum fraction cannot be lower than 0%.

Intensity-based and lifetime-based FRET Efficiency were calculated.

$$E = 1 - \frac{I_{DA}}{I_D},$$

where I_{DA} is the average nuclear intensity of the donor in presence of the acceptor from across all 3 embryos and I_D is the average nuclear intensity of the donor alone.

$$E = 1 - \frac{\tau_{DA}}{\tau_D},$$

where τ_{DA} is the average AAT of the donor in presence of the acceptor from nuclei across all 3 embryos and τ_D is the average AAT of the donor alone.

Intensity-based apparent FRET efficiency was calculated for acceptor photobleaching:

$$E_a = 1 - \frac{I_{\text{Donor+Acceptor(pre-bleach)}}}{I_{\text{Donor+Acceptor(post-bleach)}}}.$$

4.2.3 | Statistics

Mean intensity (log transformed for donor-intensity FRET and SE-FRET), and AAT were compared between conditions in R (version 4.2.1),⁴³ using linear mixed effect models (lme4, version 1.1–30) including ‘embryo’ as a random effect. The significance of pairwise comparisons between estimated marginal means was assessed with emmeans (version 1.8.0), accounting for multiple testing using the Tukey’s method.

4.2.4 | Scripts

Jupyter notebooks and R scripts used for data processing and statistics were uploaded to: <https://github.com/JuliaAuer/Auer2022—Non-fitting-FLIM-FRET-Zebrafish-embryos>

ACKNOWLEDGEMENTS

The authors would like to thank the BioImaging UK community, Dr Duncan Sproul, Dr Alessandro Brombin and Dr Wendy Bickmore for helpful discussions. Dr Elias Friman and Dr Hannes Becher for help with data analysis and statistics. The IGC Zebrafish facility, Dr Cameron Wyatt, Charli Corcoran and Johnathan Smith, and the IGC AIR facility, Matthew Pearson for technical support. Andrew Comrie and Stephen Cass for IT System management, Lindsey Marshall and Patrice Mascaldi (Leica Microsystems) for advice regarding BioImage data analysis, and Paul Cormick (Leica Microsystems) for extensive support, including early implementation of TauInteraction tools. For the kind gift of the MZnanog zebrafish line, we would like to thank Dr. Daria Onichtchouk, Developmental Biology Department, University of Freiburg.

The Stellaris 8 Equipment purchase was supported by the MRC Capital Equipment fund. J.A. was funded by a University of Edinburgh Chancellor’s Fellowship PhD studentship.

ORCID

Dong Xiao  <https://orcid.org/0000-0002-2901-9253>

Ann P Wheeler  <https://orcid.org/0000-0001-8617-827X>

REFERENCES

- Schneckenburger, H., & Richter, V. (2021). Challenges in 3D live cell imaging. *Photonics*, 8(7), 275.
- Hu, C. D., Chinenov, Y., & Kerppola, T. K. (2002). Visualization of interactions among bZIP and Rel family proteins in living cells using bimolecular fluorescence complementation. *Molecular Cell*, 9(4), 789–798.
- Wang, S., Wang, S., Ding, M., Chen, X., Chang, L., & Sun, Y. (2017). Development of bimolecular fluorescence complementation using rsEGFP2 for detection and super-resolution imaging of protein-protein interactions in live cells. *Biomedical Optics Express*, 8(6), 3119–3131.
- Forster, T. (1946). Energiewanderung und fluoreszenz. *Die Naturwissenschaften*, 33(6), 166–175.
- Stryer, L., & Haugland, R. P. (1967). Energy transfer: A spectroscopic ruler. *PNAS*, 58(2), 719–726.
- Jares-Erijman, E. A., & Jovin, T. M. (2003). FRET imaging. *Nature Biotechnology*, 21(11), 1387–1395.
- Knox, R. S., & van Amerongen, H. (2002). Refractive index dependence of the forster resonance excitation transfer rate. *The Journal of Physical Chemistry B*, 106(20), 5289–5293.

8. Halavatyi, A., & Terjung, S. (2017). Measuring molecular dynamics and interactions by Förster resonance energy transfer (FRET). In A. Wheeler, & R. Henriques (Eds.). *Standard and super-resolution bioimaging data analysis* (pp. 83–97). John Wiley & Sons Ltd.
9. Zhuo, X., & Knox, B. E. (2022). Interaction of human CRX and NRL in live HEK293T cells measured using fluorescence resonance energy transfer (FRET). *Scientific Reports*, *12*(1), 6937.
10. Zaccolo, M., De Giorgi, F., Cho, C. Y., Feng, L., Knapp, T., Negulescu, P. A., Taylor, S. S., Tsien, R. Y., & Pozzan, T. (2000). A genetically encoded, fluorescent indicator for cyclic AMP in living cells. *Nature Cell Biology*, *2*(1), 25–29.
11. Datta, R., Heaster, T. M., Sharick, J. T., Gillette, A. A., & Skala, M. C. (2020). Fluorescence lifetime imaging microscopy: Fundamentals and advances in instrumentation, analysis, and applications. *Journal of Biomedical Optics*, *25*(7), 1–43.
12. Gratton, E., Breusegem, S., Sutin, J., Ruan, Q., & Barry, N. (2003). Fluorescence lifetime imaging for the two-photon microscope: Time-domain and frequency-domain methods. *Journal of Biomedical Optics*, *8*(3), 381–390.
13. Becker, W. (2021). The bh TCSPC handbook (9th edn.). Available on www.becker-hickl.com
14. Li, D. D., Ameer-Beg, S., Arlt, J., Tyndall, D., Walker, R., Matthews, D. R., Visitkul, V., Richardson, J., & Henderson, R. K. (2012). Time-domain fluorescence lifetime imaging techniques suitable for solid-state imaging sensor arrays. *Sensors (Basel)*, *12*(5), 5650–5669.
15. Xiao, D., Sapermsap, N., Safar, M., Cunningham, M. R., Chen, Y., & Li, D. D. (2021). On synthetic instrument response functions of time-correlated single-photon counting based fluorescence lifetime imaging analysis. *Frontiers in Physics*, *9*, 635645.
16. Li, D. U., Rae, B., Andrews, R., Arlt, J., & Henderson, R. (2010). Hardware implementation algorithm and error analysis of high-speed fluorescence lifetime sensing systems using center-of-mass method. *Journal of Biomedical Optics*, *15*(1), 017006.
17. Peter, M., Ameer-Beg, S. M., Hughes, M. K., Keppler, M. D., Prag, S., Marsh, M., Vojnovic, B., & Ng, T. (2005). Multiphoton-FLIM quantification of the EGFP-mRFP1 FRET pair for localization of membrane receptor-kinase interactions. *Biophysical Journal*, *88*(2), 1224–1237.
18. Padilla-Parra, S., Auduge, N., Coppey-Moisán, M., & Tramier, M. (2011). Non fitting based FRET-FLIM analysis approaches applied to quantify protein-protein interactions in live cells. *Biophysical Reviews*, *3*(2), 63–70.
19. Digman, M. A., Caiolfa, V. R., Zamai, M., & Gratton, E. (2008). The phasor approach to fluorescence lifetime imaging analysis. *Biophysical Journal*, *94*(2), L14–6.
20. Padilla-Parra, S., Audugé, N., Coppey-Moisán, M., & Tramier, M. (2008). Quantitative FRET analysis by fast acquisition time domain FLIM at high spatial resolution in living cells. *Biophysical Journal*, *95*(6), 2976–88.
21. Roberti, M. J., Lopez, L. O., Ossato, G., Steinmetz, I., Haas, P., Hecht, F., & Alvarez, L. A. J. (2020). Application Note: TauSense: A fluorescence lifetime-based tool set for everyday imaging. *Nature Methods*, *17*(9). <https://www.nature.com/articles/d42473-020-00364-w>
22. Padilla-Parra, S., Audugé, N., Lalucque, H., Mevel, J. C., Coppey-Moisán, M., & Tramier, M. (2009). Quantitative comparison of different fluorescent protein couples for fast FRET-FLIM acquisition. *Biophysical Journal*, *97*(8), 2368–2376.
23. Alvarez, L., Roberti, J., Ossato, G., & Leica Microsystems. (2022). TauInteraction – Studying molecular interactions with TauSense. [cited 2022 14.11.2022]; Available from: <https://www.leica-microsystems.com/science-lab/life-science/tauinteraction-studying-molecular-interactions-with-tausense/>
24. Schulz, K. N., & Harrison, M. M. (2019). Mechanisms regulating zygotic genome activation. *Nature Reviews Genetics*, *20*(4), 221–234.
25. Perez-Camps, M., Tian, J., Chng, S. C., Sem, K. P., Sudhaharan, T., Teh, C., Wachsmuth, M., Korzh, V., Ahmed, S., & Reversade, B. (2016). Quantitative imaging reveals real-time pou5f3-nanog complexes driving dorsoventral mesendoderm patterning in zebrafish. *eLife*, *5*, e11475.
26. Schweikhard, V., Alvarez, L. A. J., Roberti, M. J., Birk, H., & Giske, A. (2020). Application Note: The Power HyD family of detectors for confocal microscopy. *Nature Methods*, *17*(10). <https://www.nature.com/articles/d42473-020-00398-0>
27. Verboogen, D. R. J., González Mancha, N., Ter Beest, M., & van den Bogaart, G. (2017). Fluorescence lifetime imaging microscopy reveals rerouting of SNARE trafficking driving dendritic cell activation. *eLife*, *6*, e23525.
28. Mukherjee, S., Manna, P., Hung, S. T., Vietmeyer, F., Friis, P., Palmer, A. E., & Jimenez, R. (2022). Directed evolution of a bright variant of mCherry: Suppression of nonradiative decay by fluorescence lifetime selections. *The Journal of Physical Chemistry B*, *126*(25), 4659–4668.
29. Goldman, R. D., Swedlow, J. R., & Spector, D. L. (2010). *Live cell imaging: A laboratory manual* (2nd edn.). Cold Spring Harbor Press.
30. Kimmel, C. B., Ballard, W. W., Kimmel, S. R., Ullmann, B., & Schilling, T. F. (1995). Stages of embryonic development of the zebrafish. *Developmental Dynamics*, *203*(3), 253–310.
31. Berezin, M. Y., & Achilefu, S. (2010). Fluorescence lifetime measurements and biological imaging. *Chemical Reviews*, *110*(5), 2641–2684.
32. Reisser, M., Palmer, A., Popp, A. P., Jahn, C., Weidinger, G., & Gebhardt, J. C. M. (2018). Single-molecule imaging correlates decreasing nuclear volume with increasing TF-chromatin associations during zebrafish development. *Nature Communications*, *9*(1), 5218.
33. Lukinavičius, G., Blaukopf, C., Pershagen, E., Schena, A., Reymond, L., Derivery, E., Gonzalez-Gaitan, M., D'Este, E., Hell, S. W., Wolfram, G. D., & Johnsson, K. (2015). SiR-Hoechst is a far-red DNA stain for live-cell nanoscopy. *Nature Communications*, *6*(1), 8497.
34. Laue, K., Rajshekar, S., Courtney, A. J., Lewis, Z. A., & Goll, M. G. (2019). The maternal to zygotic transition regulates genome-wide heterochromatin establishment in the zebrafish embryo. *Nature Communications*, *10*(1), 1551.
35. Tramier, M., Zahid, M., Mevel, J. C., & Masse, M. J., & Coppey-Moisán, M. (2006). Sensitivity of CFP/YFP and GFP/mCherry pairs to donor photobleaching on FRET determination by fluorescence lifetime imaging microscopy in living cells. *Microscopy Research and Technique*, *69*(11), 933–939.
36. Mitchell, C. A., Poland, S. P., Seyforth, J., Nedbal, J., Gelot, T., Huq, T., Holst, G., Knight, R. D., & Ameer-Beg, S. M.

- (2017). Functional in vivo imaging using fluorescence lifetime light-sheet microscopy. *Optics Letters*, 42(7), 1269–1272.
37. Schindelin, J., Arganda-Carreras, I., Frise, E., Kaynig, V., Longair, M., Pietzsch, T., Preibisch, S., Rueden, C., Saalfeld, S., Schmid, B., Tinevez, J. Y., White, D. J., Hartenstein, V., Eliceiri, K., Tomancak, P., & Cardona, A. (2012). Fiji: An open-source platform for biological-image analysis. *Nature Methods*, 9(7), 676–682.
38. Ollion, J., Cochennec, J., Loll, F., Escudé, C., & Boudier, T. (2013). TANGO: A generic tool for high-throughput 3D image analysis for studying nuclear organization. *Bioinformatics*, 29(14), 1840–1841.
39. van Rossum, G. (1995). Python reference manual. CWI.
40. McKinney, W. (2010). Data structures for statistical computing in python. In *9th Python in Science Conference*. Austin, Texas.
41. Harris, C. R., Millman, K. J., van der Walt, S. J., Gommers, R., Virtanen, P., Cournapeau, D., Wieser, E., Taylor, J., Berg, S., Smith, N. J., Kern, R., Picus, M., Hoyer, S., van Kerkwijk, M. H., Brett, M., Haldane, A., Del Río, J. F., Wiebe, M., Peterson, P., ... Oliphant, T. E. (2020). Array programming with NumPy. *Nature*, 585(7825), 357–362.
42. Waskom, M. L. (2021). seaborn: Statistical data visualization. *The Journal of Open Source Software*, 6(60), 3021. <https://doi.org/10.21105/joss.03021>
43. R Core Team, R. (2022). *R: A language and environment for statistical computing*. Vienna, Austria: R Foundation for Statistical Computing.

SUPPORTING INFORMATION

Additional supporting information can be found online in the Supporting Information section at the end of this article.

How to cite this article: Auer, J. M. T., Murphy, L. C., Xiao, D., Li, D. U., & Wheeler, A. P. (2023). Non-fitting FLIM-FRET facilitates analysis of protein interactions in live zebrafish embryos. *Journal of Microscopy*, 291, 43–56. <https://doi.org/10.1111/jmi.13162>